Biomech Model Mechanobiol (2014) 13:1289–1302
DOI 10.1007/s10237-014-0573-9

ORIGINAL PAPER

# Remineralization of mechanical loaded resin–dentin interface: a transitional and synchronized multistep process

**Manuel Toledano · Fátima S. Aguilera · Inmaculada Cabello · Raquel Osorio**

Received: 5 February 2014 / Accepted: 14 March 2014 / Published online: 27 March 2014


**Abstract** This study evaluated the ability of different in vitro mechanical loading tests to promote new mineral formation at bonded dentin interfaces. This research demonstrated a sequential transition in the dentin remineralizing procedure through the analysis of the mineral and matrix gradients. Mechanical loading in phosphoric acid (PA)-treated samples promoted a generalized increases in relative presence of minerals, crystallinity, ratio of phosphate peaks and a decrease in the gradient of mineral content. The organic component showed, in general terms, an increase in crosslinking. α-helices incremented in sine and square waveform loading. In EDTA + SB specimens, the relative mineral concentration incremented when loading in hold, in general. Nonuniform parameters of Bis-GMA and adhesive penetration were encountered in both groups. PA + SB promoted the highest dentin mineralization degree when loading in square, based on the increase in the relative presence of minerals and crystallinity. EDTA + SB produced any advance crystallographic maturity at the interface. High crosslinking parameters and conformational changes in proteins in PA-treated specimens indicated, indirectly, that the first remineralization is intrafibrillar.

**Keywords** Dentin · Remineralization · Load cycling · Raman analysis

## 1 Introduction

Dentin can be regarded as a biological composite with organic and inorganic components (Marshall et al. 1997). The dentin organic matrix is mainly constituted of collagen type I contributing to the biomechanical and functional properties of the tissue (Daood et al. 2013). Current dentin bonding strategies rely on micromechanical retention and chemical absorption between collagen and infiltrated resin in the demineralized dentin layer. This interface has been called a resin-reinforced or hybrid layer (HL), made of resin and collagen (Nakabayashi 1992; Wang and Spencer 2003), and it is supposed to be the weakest link in the adhesive–dentin bond (Sano et al. 1999; Erickson 1992). The formation of HL is not completely achieved under clinical conditions (Wang and Spencer 2003), leaving exposed collagen fibrils at the bottom of this resin-matrix layer (BHL), especially with the adhesives to be applied in acid-treated dentin surfaces. "Etch-and-rinse" adhesives represent the golden standard in adhesive dentistry and involve a separate etch-and-rinse phase before the application of the adhesive. In their most common configuration, an acid (phosphoric acid/PA or ethylenediaminetetraacetic acid/EDTA) is applied, to demineralize the underlying dentin (De Munck et al. 2005; Osorio et al. 2005), and then, rinsed off. This conditioning step is followed by a priming step and application of the adhesive resin. It has been demonstrated (Toledano et al. 2012a) a stronger dentin-demineralization effect of PA compared with EDTA, that will lead, consequently, to a higher volume of demineralized/unprotected collagen, at the bottom of the hybrid layer (BHL) (Xu and Wang 2012). This vulnerable unsupported collagen may become the sites for collagen hydrolysis by host-derived matrix metalloproteinase (MMP) enzymes (Toledano et al. 2012b).

Teeth are continuously subjected to stresses during mastication, swallowing and parafunctional habits (Frankenberger et al. 2005). In general, bruxism is defined as a diurnal or nocturnal parafunctional activity that includes clenching (continuous or sustained loading), bracing, gnashing and grinding

M. Toledano (✉) · F. S. Aguilera · I. Cabello · R. Osorio
Faculty of Dentistry, Dental Materials Section, University of Granada, Colegio Máximo de Cartuja s/n, 18071 Granada, Spain
e-mail: toledano@ugr.es

of teeth, in other than chewing (cyclid loading) movement of mandible. The range and duration of loading and the pattern of cycling loading may be intended to include physiologically realistic patterns of chewing and clenching. Occlusal trauma is caused by conditions such as premature contacts, bruxism and clenching (Noma et al. 2007) and can affect both restorations and restorative strategies involving dentin. Thereby, minimally invasive dentistry encompasses the philosophy of preservation of the maximum quantity of reparable dental tissues and utilizing remineralization approaches (Simonsen 1987), to obtain the integrity of the resin–dentin interface. Additionally, it has been demonstrated that in vitro load cycling promoted mineralization at the resin-infiltrated dentin and mineral depleted areas of the resin–dentin interface, at 24 h and 3 weeks of storage (Toledano et al. 2014a,b).

Confocal Raman spectroscopy analysis is used as a quantitative chemical assessment methodology for biological samples in conjunction with the fact that the Raman peak intensity is proportional to the number of molecules within the volume of the scanned area (Milly et al. 2014). It is a nondestructive and sensitive method capable of identifying individual spectral bands arising from the inorganic calcium phosphate crystals and the protein/lipid constituents of dentin (Wang et al. 2009). Micro-Raman mapping technique appeared to offer a powerful method to directly analyze the resin–dentin interface and the mineral content and distribution after the adhesive procedure and stimuli. Various methods of multivariate analysis (Toledano et al. 2014a, Almahdy et al. 2012), such as principal component analysis (PCA) and clustering k-means (KMC), have been established for analyzing two-dimensional *data*.

In this in vitro study, we attempted to clarify the morpho-chemical influence of chewing and clenching on the resin–dentin interface. The purpose of this study was to evaluate the ability of different in vitro mechanical loading tests to promote transitional morpho-chemical changes and to induce new mineral formation on the bonded dentin interface created using two different demineralization procedures before the adhesive application. The tested null hypothesis is that a transitional and synchronized procedure of new mineral formation is not produced at the resin–dentin interface after in vitro mechanical loading tests.

## 2 Material and methods

### 2.1 Specimen preparation, bonding procedures and mechanical loading tests

Twenty noncarious human third molars were obtained with informed consent from donors (20–40 years of age), under a protocol approved by the Institution Review Board. Molars were stored at 4°C in 0.5 % chloramine T for up to 1 month before use. A flat mid-coronal dentin surface was exposed using a hard tissue microtome (Accutom-50; Struers, Copenhagem, Denmark) equipped with a slow-speed, water-cooled diamond wafering saw (330-CA RS-70300, Struers, Copenhagen, Denmark). A 180-grit silicon carbide (SiC) abrasive paper mounted on a water-cooled polishing machine (LaboPol-4, Struers, Copenhagem, Denmark) was used to produce a clinically relevant smear layer (Koibuchi et al. 2001). The specimens were divided into two main groups (n = 10) based on the tested adhesive systems and dentin-etching procedure: (i) two-step etch&rinse adhesive system, Adper™ Single Bond Plus (SB, 3M ESPE, St. Paul, MN, USA) applied on 37 % phosphoric acid (PA) etched dentin, 15 s (PA + SB); (ii) SB applied on EDTA-treated dentin, 0.5M, pH 7.4, 60s (EDTA + SB). A flowable resin composite (Tetric EvoCeram® -Ivoclar Vivadent, Schaan, Liechtenstein-) was placed incrementally in five 1 mm layers and light cured with a Translux EC halogen unit (Kulzer GmbH, Bereich Dental, Wehrheim, Germany) for 40s. The detailed composition and application mode is shown in Table 1.

The specimens were divided into five subgroups, based on the type of mechanical loading that applied: (1) restored teeth storage in simulated body fluid (SBF), for 24 h (unloaded), (2) load cycling with sine waveform (259,459 cycles, 3 Hz,) (S-MMT-250NB; Shimadzu, Tokyo, Japan), (3) load cycling with square waveform (6,171 cycles, 0.072 Hz,) (S-MMT-250NB; Shimadzu, Tokyo, Japan), (4) load with hold waveform, for 24 h (Instron 3345, Instron Corporation, Canton, MA, USA) and (5) load with hold waveform, for 72 h (Instron 3345, Instron Corporation, Canton, MA, USA). To proceed with the mechanical loaded samples, specimens were mounted in plastic rings using dental stone. The compressive load of 225 N was applied to the flat resin composite buildups using a 5-mm diameter spherical stainless steel plunger, while immersed in SBF (Sauro et al. 2009). All specimens were longitudinally sectioned in 1.5-mm slabs from the central part of the specimen and polished through SiC abrasive papers from 800 up to 4,000-grit with a final polishing procedure performed with diamond pastes (Buehler-MetaDi, Buehler Ltd. through 1 μm down to 0.25 μm. The specimens were treated in ultrasonic bath (Model QS3, Ultrawave Ltd, Cardiff, UK) containing deionized water [pH 7.4] for 5 min at each polishing step.

### 2.2 Raman spectroscopy and cluster analysis

A dispersive Raman spectrometer/microscope (Horiba Scientific Xplora, Villeneuve d'Ascq, France) was also used to analyze bonded interfaces. A 785-nm diode laser (100 mW sample power) through a ×100/0.90 NA air objective was employed. Raman signal was acquired using a 600-lines/mm grating centered between 900 and 1, 700 $cm^{-1}$. Chemical mapping of the interfaces was performed. A 45μm × 45μm

**Table 1** Composition and application mode of etchants and adhesive resin

| Dentin conditioning | Resin composition Single bond (3M ESPE, USA) | Application procedure |
|---|---|---|
| 37 % $H_3PO_4$ (15 s) | HEMA | Dentin conditioning |
| or | Bis-GMA | Rinse with water |
| 0.5 M EDTA (60 s) | Ethanol | Air-dry (5 s) |
| | PAM | Adhesive application (30 s) |
| | UDMA | Light activation (15 s) |
| | CQ | |
| | ODMAB | |
| | Tripheylantimonydicaroxylates | |
| | Phosphine | |
| | Water | |
| | Quartz | |

*EDTA* ethylenediaminetetraacetic acid, *Bis-GMA* bisphenol A diglycidyl methacrylate, *HEMA* 2-hydroxyethyl methacrylate, *CQ* camphorquinone, *ODMAB* 2-(ethylhexyl)-4-(dimethylamino)benzoate(co-initiator), *PAM* polyacrylic acid methacrylated, *UDMA* urethane dimethacrylate, *MDP* methacryloyldodecylphosphate

area of the interfaces was mapped using 2 μm spacing at X axis and 1 μm at Y axis. A total of 1,100 points were performed per map. The resolution of the mapping was 6.25 $cm^{-1}$. The size of the RAMAN map compared to the size of the resin–dentin interface was 1:1 when using a 100× objective. BHL depth was between 0.25 and 2.25 μm and HL ranged from 2.00 μm to 6.00 μm approximately (Fig. 1). Gaussian–lorentzian peaks summed to match small regions of the spectrum were obtained by a nonlinear peak-fitting routine that employs the Levenberg–Marquardt algorithm and a first-order polynomial (Milly et al. 2014, Awonusi et al. 2007).

K-means cluster (KMC) analysis was executed using the multivariate analysis tool (ISys® Horiba), as hypotheses concerning the number of clusters formed in resin-bonded interfaces were previously obtained (Toledano et al. 2014a,b). However, Ward's method was employed to get some sense of the number of clusters and the way they merge as seen from the dendrogram. Clusters were created following Ward's technique, and the dendrogram was calculated applying five to six factor spectra (principal components). The aim of a factor analysis lies in the effective reduction in the dataset dimension while maintaining a maximum of information. This method was used to model the data and to determine spectral variances associated for data differentiation. It resulted in the calculation of a new coordinate system whereby variations of the dataset is described via new axes, principal components (PC). The K-means clustering is a method of cluster analysis based on a centroid model which aims to partition *n* observations into *k* clusters in which each observation belongs to the cluster with the nearest mean (Almahdy et al. 2012). The natural groups of components (or *data*) based on some similarity and the centroids of a group of *data* sets were found by the clustering algorithm once calculated by the software. To determine the chemical cluster similarity, this algorithm evaluated the distance between a point and the cluster centroids. The output from a clustering algorithm was basically a statistical description of the cluster centroids with the number of components in each cluster. The biochemical content of each cluster was analyzed using the average cluster spectra. Five to six clusters were identified, and values for each cluster such as hybrid layer, dentin and adhesive within the interface were independently obtained. Principal component analysis (PCA) decomposed *data* set into a bilinear model of linear independent variables, the so-called principal components ($PC_S$). Two principal components were selected for the present study at interfaces: hybrid layer (HL) and bottom of hybrid layer (BHL). In the unloaded specimens, PCs concerning to adhesive (ADH) and dentin (DEN) were also included, to provide values for reference and calculations. As the cluster centroids are essentially means of the cluster score for the elements of cluster, the mineral and organic components of dentin hybrid layers were examined for each cluster, trough the following parameters.

The mineral component of dentin was analyzed examining the following parameters (Toledano et al. 2013):

*Relative presence of mineral:*

1. *Phosphate* (960 $cm^{-1}$) *and carbonate* (1,070 $cm^{-1}$) *peaks and areas of their bands.* Peak heights were processed in absorbance units.
2. *Relative mineral concentration* (i.e., mineral-to-matrix ratio): It was inferred from the visible ratio of the intensities of the peaks at 960 $cm^{-1}$ (phosphate) ($PO_4^{3-}$) and 1,003 $cm^{-1}$ (phenyl group), the aromatic ring of phenylalanine residues in collagen or peaks at 1,070 $cm^{-1}$ (carbonate) ($CO_3^{2-}$) and 1,003 $cm^{-1}$. These indexes concerned with the maximum relative degree of mineralization (Schwartz et al. 2012; Karan et al. 2009). Additionally, peaks at 960 $cm^{-1}$ and 1,450 ($CH_2$) or 1,070 $cm^{-1}$ and 1,450 can be used (Wang et al. 2009).

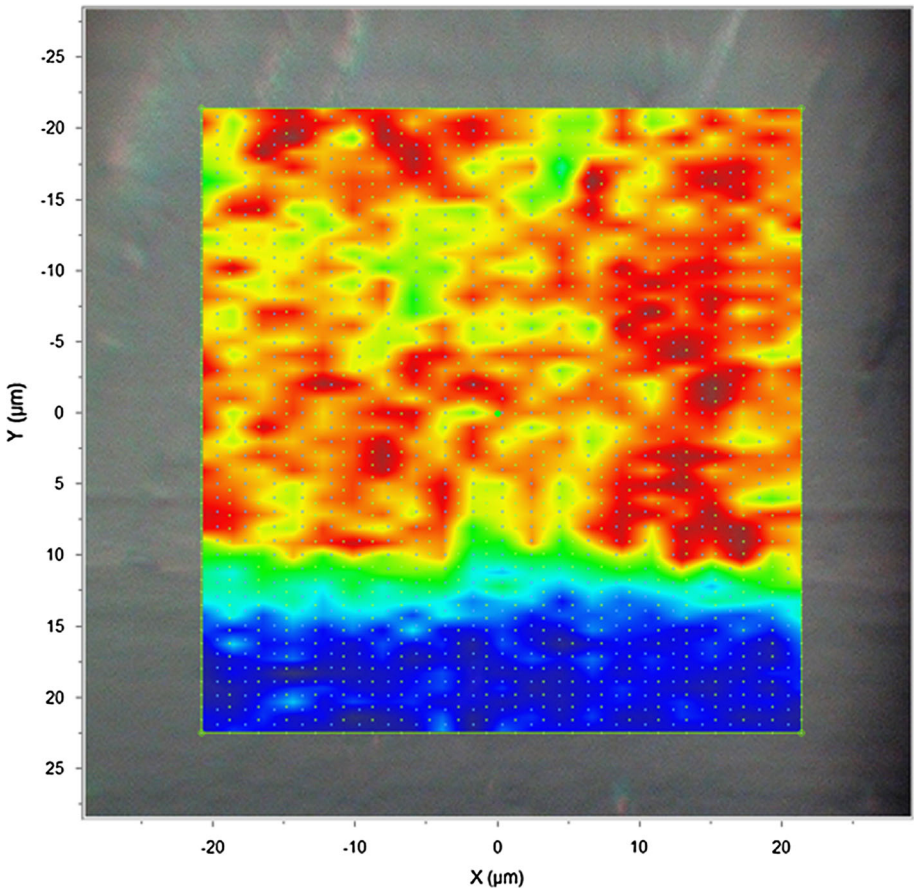


**Fig. 1** 2D micro-Raman map at the resin–dentin-bonded interface on the 50 µm × 50 µm optical image at 100×

*Crystallinity*: It was evaluated based on the full width at half maximum (FWHM) of the phosphate band at 960 $cm^{-1}$ and carbonate band at 1,070 $cm^{-1}$. These indexes expressed the crystallographic or relative atomic order, since narrower peaks suggest less structural variation in bond distances and angles (Schwartz et al. 2012). In general, the narrower the spectral peak width is, the higher the degree of mineral crystallinity (Karan et al. 2009).

*Gradient in mineral content* or carbonate content of the mineral crystallites: It was assessed as the relationship between the ratio of heights at 1,070 $cm^{-1}$ (carbonate) ($CO_3^{2-}$) and 960 $cm^{-1}$ (phosphate) ($PO_4^{3-}$), indicating carbonate substitution for phosphate (Schwartz et al. 2012).

*Phosphate peaks ratio*: It assesses the ratio between the mineral peak at 960 $cm^{-1}$ (phosphate) ($PO_4^{3-}$), within the demineralized zone, and the mineral peak ($PO_4^{3-}$) within the healthy substratum (Milly et al. 2014).

The organic component of dentin was analyzed examining the following parameters:

*Normalization:* Phenyl group: The peak at 1,003 $cm^{-1}$, which is assigned to C–C bond in the phenyl group, was used for normalization (Xu and Wang 2011).

*Crosslinking:*

1. Pyridinium ring vibration: In the spectra, the peak appeared at 1,030/1,032.7 $cm^{-1}$, is assigned to the C–C in pyridinium ring vibration which has a trivalent amino acid crosslinking residue (Daood et al. 2013). The relative intensity of this peak increases after the crosslinking formation (Jastrzebska et al. 2003).
2. Ratio pyridinium/phenyl (1,031 $cm^{-1}$/1,001 $cm^{-1}$): the higher the ratio, the greater the extend of collagen crosslinking (Xu and Wang 2012; Jastrzebska et al. 2003).
3. Ratio 1660 (amide I)/1690–1701: decreases when mineralization increases.
4. Ratio 1004 (phenyl)/1450 ($CH_2$): arises preceding deposition of HAP (hydroxyapatite) crystals within the structure (Wang et al. 2009).

*Nature of collagen:*

1. Amide III, CH and amide I: The peaks at 1246/1270, 1450 and 1,655/1,667 $cm^{-1}$, assigned to amide III, CH

and amide I, respectively, are sensitive to the molecular conformation of the polypeptide chains (Xu and Wang 2011; Jastrzebska et al. 2003).
2. Amide I peak: The decrease indicates damage or removal of collagen fibrils (Xu and Wang 2012).
3. Ratio amide I/amide III concerned the organization of collagen.
4. 1,340 $cm^{-1}$ peak: This signal has been assigned to protein α-helices where intensity is sensitive to molecular orientation (Wang et al. 2009).

Degree of adhesive efficacy:

*Degree of conversion of adhesive*: Ratio 1637/1608. The peak appearing at 1,637 $cm^{-1}$ is associated with C=C of methacrylate, and the peak at 1,608 $cm^{-1}$ is related to C–C in phenyl of adhesive monomer (Xu and Wang 2012).
*Bis-GMA penetration*: Ratio 1113/1667. The peak appearing at 1,113 $cm^{-1}$ is associated with C–O–C of adhesive, and the peak at 1,667 $cm^{-1}$ is related to amide I (Wang and Spencer 2003; Xu and Wang 2012).
*Adhesive (Bis-GMA and HEMA) penetration*: Ratio 1454/1667. The peak appearing at 1,454 $cm^{-1}$ is assigned to the $CH_2$ group of both Bis-GMA and HEMA, and the peak at 1,667 $cm^{-1}$ is related to amide I (Wang and Spencer 2003; Xu and Wang 2012).
*Others*: The peak at 1,720 $cm^{-1}$ is associated at carbonyl group. The peak at 1,453 $cm^{-1}$ is associated at $CH_2$ def (Wang and Spencer 2003; Xu and Wang 2012).

## 3 Results and discussion

Dentin is a composite material containing mineral nanocrystallites and a protein matrix that is predominantly crosslinked type I collagen. The mineral is a carbonated calcium phosphate within the apatite crystallite structure group (Awonusi et al. 2007).

Contemporary dental restorative techniques usually employ a dentin bonding step in order to create a stable connection between composite resin and intact dentin. This study aimed to assess the effect of cyclic and sustained mechanical loading on remineralization of resin–dentin interfaces created with an etch-and-rinse adhesive. Two different dentin-etching procedures (PA vs. EDTA) were used, and Raman cluster analysis/PCA-KMC was employed to chemically assess the resin–dentin interface.

Load cycling can be undertaken following a standard pattern of load (sine waveform) (Toledano et al. 2014a) or following bruxism events (square waveform) (Nishigawa et al. 2001). This squared function may be converted into constant lineal and sustained function by holding permanently up some limit certain force, in order to prolong the maximum trajectory, temporally (24 vs. 72 h), of this clenching effect. Cycling loading of 259,200/3 Hz (load cycling sine) or 6,171/0.072 Hz (load cycling square) for 24 h and mechanical loading in hold (24 and 72 h) are greatest in excess of normal or parafunctional patterns. In the present study, three clenching levels have been reproduced (waveforms square and hold 24 and 72 h).

This study dealt, firstly, with the degree of mineralization, i.e., mineral-to-matrix ratios (Schwartz et al. 2012), related to phosphate and carbonate. Plots of both ratios, in PA + SB, confirmed the higher relative degree of mineralization after mechanical loading. Loading in square attained the maximum ratio concerning the phosphate peak at both HL (28.93) and BHL (37.8) (Fig. 2c), ∼ 12- and 11-folds, respectively, the values attained in the unloaded specimens (Table 2) (Fig. 2a). The Raman phosphate peak at 950 $cm^{-1}$ characterizes tetrahedral $PO_4$ group (P-O bond) within hydroxyapatite (HAP). Monitoring the intensity of this peak has been used to assess the potential increase in phosphate content (Milly et al. 2014).

When carbonate peak was considered, similarly, the maximum values were obtained in the square waveform at both HL (3.38) and BHL (5.38), approximately fivefolds, respectively (Fig. 2a, c), the data in the unloaded samples (Table 2). The increment in mineral-to-matrix ratio did not correlated well with a similar augmentation in nanomechanical properties localized at these sites (Toledano et al. 2014c). Loading square produced ∼ 50 % lower Young's modulus values than loading hold 72 h at both HL and BHL. Loading square showed a phosphate peak (60.46) lower than loading hold 72 h at HL (41.29) (Table 2). On the contrary, the 1,003 $cm^{-1}$ band (assigned to phenylalanine) which was used to calculate the RMC was bigger in loading hold 72 h (3.76) (Fig. 2e) than in loading square (2.09), at HL (Tables 2, 3). Considering that the improvement of Young's modulus is associated with a remineralizing effect (Toledano et al. 2014c,d), it can be assumed that the degree and quality of mineralization (Balooch et al. 2008) is proximately twofold in loading hold 72 h (lower peak and area of P) than in square (higher peak and area of P). The decrease in 1,003 $cm^{-1}$ signal (∼ 43 and ∼ 27 % at both HL and BHL, respectively), consistently preceded the dramatic rise in mineral content (Wang et al. 2009) (Tables 2, 3). Though the relative mineral content (RMC) is higher in loading square than in loading hold 72 h, the most favorable mechanical performance found in loading hold (Toledano et al. 2014d) insures that the effective dentin mineralization is intrafibrillar. Indeed, the formation of a surface layer of mineral (e.g., loading in square) is not a sufficient event to produce high Young's modulus values, as the extrafibrilar minerals act as a granular material that can withstand load, but in the absence of intrafibrillar mineralization, the capacity to sustain load in hydrated status is quite low (Kinney et al. 2003). Thereby, intrafibrillar mineralization is a key factor to ensuring that collagen fibrils have the

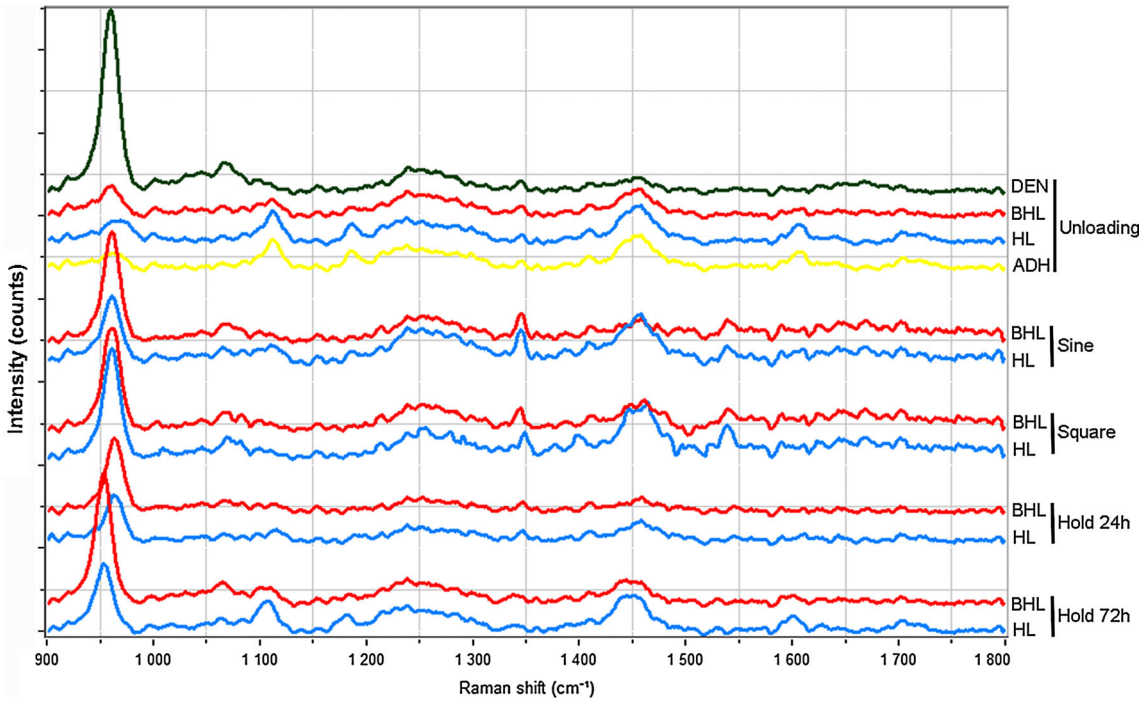


**Fig. 2** PA + SB. **a** Unloaded specimen. **b** Loaded in sine waveform specimens. **c** Loaded in square waveform specimens. **d** Loaded in hold 24 h waveform specimens. **e** Loaded in hold 72 h waveform specimens. Raman spectra of principal components (PCs): *ADH* adhesive; *HL* hybrid layer; *BHL* bottom of hybrid layer; *DEN* dentin

**Table 2** Mineral gradients in phosphoric acid (PA)-treated dentin surfaces plus single bond (SB) adhesive application (PA + SB)

| | Relative presence of mineral | | | | | | FWHM | | GMC ratio C/P | PPR ratio phosphate peak/healthy substratum |
|---|---|---|---|---|---|---|---|---|---|---|
| | Phosphate [961] | | | Carbonate [1070] | | | Phosphate | Carbonate | | |
| | Peak | Area | RMC | Peak | Area | RMC | | | | |
| *Unloaded* | | | | | | | | | | |
| ADH | 9.09 | 259.95 | 2.98 | 3.11 | 51.37 | 0.98 | 22.56 | 12.65 | 0.34 | 0.08 |
| HL | 13.65 | 444.4 | 2.38 | 4.16 | 68.79 | 0.73 | 25.70 | 12.65 | 0.30 | 0.12 |
| BHL | 18.46 | 527 | 3.45 | 6.08 | 125.33 | 1.14 | 22.52 | 15.82 | 0.33 | 5.96 |
| DEN | 109.99 | 2,704.94 | 14.17 | 17.93 | 870.92 | 2.31 | 19.31 | 37.86 | 0.16 | 1 |
| *Sine* | | | | | | | | | | |
| HL | 39.86 | 980.82 | 8.12 | 8.86 | 182.61 | 1.8 | 19.30 | 15.82 | 0.22 | 0.36 |
| BHL | 67.43 | 1,390.57 | 10.62 | 14.86 | 306.29 | 2.34 | 16.09 | 15.81 | 0.22 | 0.61 |
| *Square* | | | | | | | | | | |
| HL | 60.46 | 1,495.32 | 28.93 | 7.06 | 482.31 | 3.38 | 19.28 | 53.87 | 0.12 | 0.55 |
| BHL | 58.60 | 1,211.5 | 37.8 | 8.34 | 171.365 | 5.38 | 16.04 | 15.76 | 0.14 | 0.53 |
| *Hold 24 h* | | | | | | | | | | |
| HL | 28.3 | 697.81 | 11.74 | 4.99 | 82.53 | 2.07 | 19.33 | 12.65 | 0.17 | 0.26 |
| BHL | 44.37 | 1,094.02 | 14.74 | 6.64 | 163.86 | 2.2 | 19.33 | 18.98 | 0.15 | 0.4 |
| *Hold 72 h* | | | | | | | | | | |
| HL | 41.29 | 1,173.74 | 10.98 | 8.18 | 463.13 | 2.18 | 22.55 | 44.35 | 0.19 | 0.38 |
| BHL | 79.12 | 1,939.97 | 16.91 | 13.06 | 374.48 | 2.79 | 19.33 | 22.11 | 0.16 | 0.72 |

*RMC* relative mineral concentration between mineral/phenyl (1003), *FWHM* full-width half-maximum, *GMC ratio C/P* gradient in mineral content between carbonate and phosphate peak, *PPR* phosphate peaks ratio, *ADH* adhesive, *BHL* bottom of hybrid layer, *HL* hybrid layer, *DEN* dentin, peaks positions are expressed in $cm^{-1}$

**Table 3** Organics and adhesive gradients in phosphoric acid (PA)-treated dentin surfaces plus single bond (SB) adhesive application (PA + SB)

| | Normalization Organics | | | | | | | | | Adhesive | | | | |
|---|---|---|---|---|---|---|---|---|---|---|---|---|---|---|
| | Crosslinking | | | | | Nature of collagen | | | | α-helices [1340] | DC [1637/1608] | Bis-GMA penetration [1113/amide I] | Adhesive penetration [1453/1667] | 1720 | 1453 |
| | Phenyl [1003] | Pyrid. [1032] | Ratio [1031/1001] | Ratio [1660/1690] | Ratio phenyl/$CH_2$ [1003/CH] | A-III [1246–1270] | CH [1450] | A-I [1655–1667] | Ratio amide I/amide III | | | | | | |
| *Unloaded* | | | | | | | | | | | | | | | |
| ADH | 3.05 | 1.89 | 0.62 | 0.19 | 0.15 | 13.79 | 19.76 | 1.18 | 0.08 | 4.01 | 0.36 | 14.50 | 16.74 | 4.95 | 19.76 |
| HL | 5.73 | 3.20 | 0.55 | 0.22 | 0.26 | 14.96 | 22.45 | 1.42 | 0.09 | 4.46 | 0.37 | 13.29 | 15.8 | 5.50 | 22.45 |
| BHL | 5.35 | 5.53 | 1.03 | 0.84 | 0.33 | 14.97 | 16.25 | 3.58 | 0.24 | 5.99 | 0.90 | 2.78 | 4.54 | 2.34 | 16.25 |
| DEN | 7.76 | 10.64 | 1.37 | 1.5 | 0.99 | 15.02 | 7.82 | 6.36 | 0.42 | 6.35 | 2.83 | 1.21 | 1.23 | 1.37 | 7.82 |
| *Sine* | | | | | | | | | | | | | | | |
| HL | 4.91 | 5.26 | 1.07 | 1.02 | 0.17 | 20.04 | 29.02 | 9.12 | 0.45 | 19.33 | 1.21 | 1.14 | 3.18 | 5.93 | 29.02 |
| BHL | 6.35 | 13.11 | 2.06 | 0.96 | 0.34 | 20.13 | 18.55 | 17.20 | 0.85 | 20.53 | 1.28 | 0.57 | 1.08 | 14.08 | 18.55 |
| *Square* | | | | | | | | | | | | | | | |
| HL | 2.09 | 5.89 | 2.81 | 1.00 | 0.08 | 22.34 | 26.45 | 10.61 | 0.40 | 8.61 | 3.59 | 0.69 | 2.49 | 7.61 | 26.45 |
| BHL | 1.55 | 1.07 | 0.69 | 0.58 | 0.12 | 15.88 | 12.47 | 5.21 | 0.32 | 6.50 | 3.84 | 0.71 | 2.39 | 3.0 | 12.47 |
| *Hold 24 h* | | | | | | | | | | | | | | | |
| HL | 2.41 | 3.48 | 1.44 | 0.44 | 0.19 | 10.03 | 12.87 | 2.07 | 0.20 | 6.63 | 0.83 | 3.56 | 6.21 | 3.28 | 12.87 |
| BHL | 3.01 | 5.08 | 1.69 | 0.57 | 0.35 | 8.36 | 8.61 | 1.76 | 0.21 | 5.89 | 1.49 | 2.59 | 4.89 | 1.24 | 8.61 |
| *Hold 72 h* | | | | | | | | | | | | | | | |
| HL | 3.76 | 4.53 | 1.20 | 0.25 | 0.17 | 15.74 | 21.91 | 1.75 | 0.11 | 3.99 | 0.45 | 10.59 | 12.52 | 4.64 | 21.91 |
| BHL | 4.68 | 7.33 | 1.56 | 0.58 | 0.33 | 15.0 | 14.40 | 2.58 | 0.17 | 5.34 | 0.63 | 3.86 | 5.58 | 2.39 | 14.40 |

*Pyrid.* pyridinium, *DC* degree of conversion of adhesive, *A-* amide, *ADH* adhesive, *BHL* bottom of hybrid layer, *HL* hybrid layer, *DEN* dentin. Peaks positions are expressed in $cm^{-1}$

**Table 4** Mineral gradients in EDTA-treated dentin surfaces plus Single Bond (SB) adhesive application (EDTA + SB)

| | Relative presence of mineral | | | | | | FWHM | | GMC ratio C/P | PPR ratio phosphate peak/healthy substratum |
|---|---|---|---|---|---|---|---|---|---|---|
| | Phosphate [961] | | | Carbonate [1070] | | | Phosphate | Carbonate | | |
| | Peak | Area | RMC | Peak | Area | RMC | | | | |
| *Unloaded* | | | | | | | | | | |
| ADH | 9.99 | 363.8 | 2.79 | 4.08 | 84.07 | 1.14 | 29 | 15.81 | 0.4 | 0.08 |
| HL | 43.67 | 1,073.74 | 12.44 | 7.48 | 184.57 | 2.13 | 19.31 | 18.98 | 0.17 | 0.34 |
| BHL | 84.61 | 2,080.5 | 17.73 | 12.87 | 317.45 | 2.7 | 19.31 | 18.98 | 0.15 | 0.67 |
| DEN | 125.85 | 30.94.5 | 16.56 | 18.95 | 845.66 | 2.49 | 19.3 | 34.7 | 0.15 | 1 |
| *Sine* | | | | | | | | | | |
| HL | 45.74 | 1,304.83 | 3.04 | 13.02 | 268.48 | 0.87 | 22.52 | 15.82 | 0.28 | 0.36 |
| BHL | 83.40 | 2,051.1 | 15.59 | 13.15 | 271.02 | 2.45 | 19.3 | 15.82 | 0.15 | 0.66 |
| *Square* | | | | | | | | | | |
| HL | 15.49 | 442.17 | 5.49 | 4.61 | 76.13 | 1.63 | 22.52 | 12.65 | 0.29 | 0.12 |
| BHL | 37.93 | 933.45 | 16.42 | 6.71 | 165.61 | 2.9 | 19.3 | 18.98 | 0.17 | 0.30 |
| *Hold 24 h* | | | | | | | | | | |
| HL | 70.74 | 1,740.62 | 16.18 | 11.5 | 330.22 | 2.63 | 19.3 | 22.15 | 0.16 | 0.56 |
| BHL | 152.34 | 3,752.41 | 25.01 | 21.31 | 940.63 | 3.5 | 19.34 | 34.31 | 0.14 | 1.21 |
| *Hold 72 h* | | | | | | | | | | |
| HL | 64.24 | 1,579.74 | 18.2 | 9.4 | 231.95 | 2.66 | 19.31 | 18.98 | 0.14 | 0.51 |
| BHL | 126.43 | 3,109.2 | 22.1 | 17.13 | 653.69 | 2.99 | 19.31 | 29.55 | 0.13 | 1.01 |

*RMC* relative mineral concentration between mineral/Phenyl (1003), *FWHM* full-width half-maximum, *GMC ratio C/P* gradient in mineral content between carbonate and phosphate peak, *PPR* phosphate peaks ratio, *ADH* adhesive, *BHL* bottom of hybrid layer, *HL* hybrid layer, *DEN* dentin. Peaks positions are expressed in $cm^{-1}$

same high modulus of elasticity as occurs in natural biomineralized dentin (Balooch et al. 2008). Nevertheless, loading square samples exhibited greater crystallographic maturity than loading hold 72 h, i.e., it showed lower degree of imperfections.

The term crystallinity refers to the order of a solid where a highly crystalline material displays long range order among its component atoms and amorphous material. The extent of crystallinity can vary in two ways: the order of the component atoms can become more or less perfect, and the overall size of individual crystals can change (Wang et al. 2009). The narrowing of the phosphate $v_1$ peak (at ca. 960 $cm^{-1}$) (i.e., lower FWHM or higher relative crystallinity), at both HL ($\sim$ 20 %) and BHL ($\sim$ 23 %), as the carbonate content increased (GMC) was shown in all loading tests, when PA was used as etching agent, and observed in Table 2 and Fig. 2a–e. On the contrary, when EDTA + SB were evaluated, crystallinity did not change or diminished (HL in loading in sine and square) (Table 4) (Fig. 3a–e). The increment in crystallinity has been attributed (Awonusi et al. 2007; Krajewski et al. 2005) to an increase in crystallographic perfection in the apatite unit cell as carbonate substituted for phosphate. At HL, in PA + SB, the lowest crystallographic maturity was attained in hold 72 h (22.55) (Fig. 2e), suggesting the presence of small hydroxyapatite crystals exhibiting a relative higher degree of imperfection and substitution than the other loading tests, but still less than the unloaded specimens (25.70). Raman spectroscopy in PA + SB unloaded (Fig. 2a) showed, at HL, a double peak (955–960 $cm^{-1}$) at phosphate shift, probably representing an intermediate mineral crystal poorly carbonated apatite, octa-calcium phosphate-like phase, characterized on a Raman band at 955 $cm^{-1}$ (Wang et al. 2009). On the other hand, FWHM relative to carbonates in PA + SB exhibited a decrease in crystallinity in all loading tests at HL (except hold 24 h) and in hold at BHL. This crystallographic perfection was inferior (maximum FWHM) in hold 72 h (Table 2; Fig. 2e). In EDTA + SB specimens, FWHM relative to carbonates performed dissimilar, displaying increments (e.g., square at HL, Fig. 3c), decrements (e.g., hold 24 h at HL, Fig. 3d) or unchanged (e.g., hold 72 h at HL, Fig. 3e).

On the contrary, when EDTA + SB specimens were analyzed, the phosphate peak incremented when loading in hold ($\sim$ 38 %), attaining the maximum value of RMC at HL, in hold 72 h (18.2), and at BHL, in hold 24 h (25.01) (Table 4). The carbonate concentration in calcified tissue provides valu-

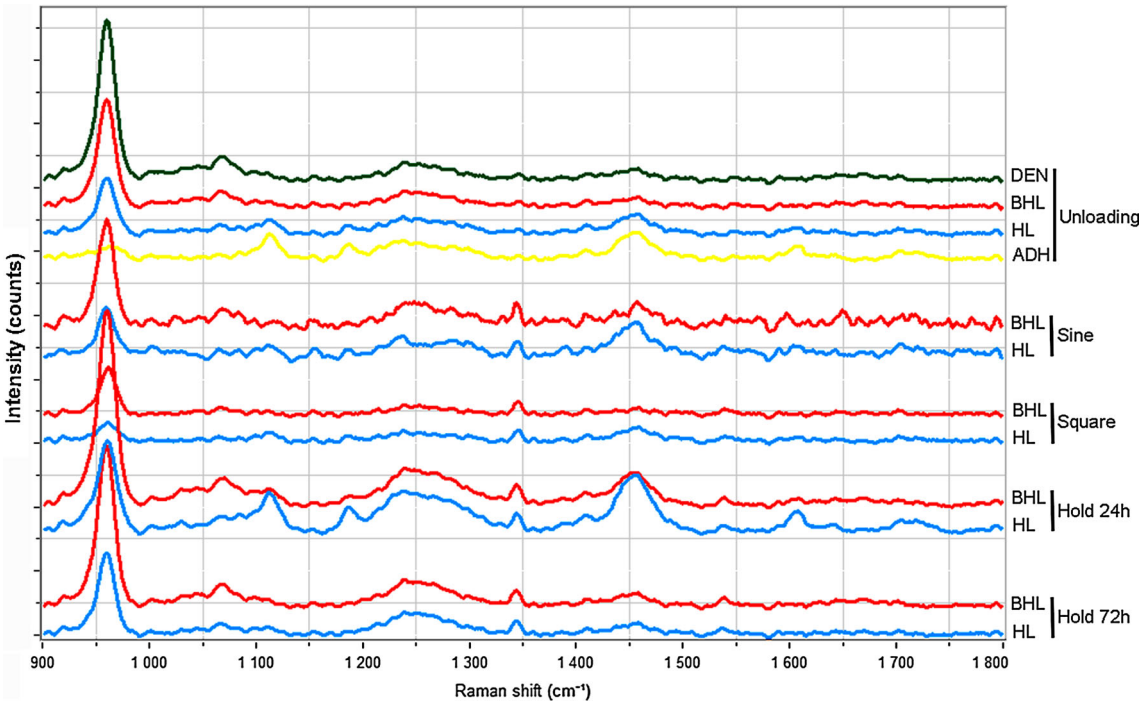


**Fig. 3** EDTA+SB. **a** Unloaded specimen. **b** Loaded in sine waveform specimens. **c** Loaded in square waveform specimens. **d** Loaded in hold 24 h waveform specimens. **e** Loaded in hold 72 h waveform specimens. Raman spectra of principal components (PCs): *ADH* adhesive; *HL* hybrid layer; *BHL* bottom of hybrid layer; *DEN* dentin

able information and varies with maturity and crystallinity. The presence of B-type carbonate in apatite has been associated with Raman band at ca. 1,070–1,073 $cm^{-1}$. The carbonate $\upsilon_1$ peaks found at 1,070 $cm^{-1}$, and its height and area are strongly associated with weight percent carbonate in the apatite (Awonusi et al. 2007). The relative mineral concentration (MRC) concerning the carbonate peak increased after mechanical loading stimuli ($\sim$ 38 %, at HL in sine) and followed similar trend than phosphate (Table 4). Additionally, loading in hold 24 h showed a reduced symmetry in undistorted trigonal planar carbonate in the crystal lattice, which caused two $CO_4^{3-}$ peaks (Fig. 3d). This splitting effect into two bands has concerned some changes in this spectral region with carbonate content, ascribed to either growth of a carbonate peak or changes in the phosphate peak in response to the presence of carbonate in the lattice, as the 1,071 $cm^{-1}$ peak is a superposition of carbonate $\upsilon_1$ and phosphate $\upsilon_3$, which can be linearly correlated with the carbonate content of the apatite (Awonusi et al. 2007). These findings imply not only an increase in both phosphate and carbonate area when loading, but a reduction in the phenyl peak (1,003 $cm^{-1}$) in similar conditions (Table 3) (Karan et al. 2009), in the specimens treated with PA (Table 3). When EDTA was used for dentin etching, a general increase at 1,003 $cm^{-1}$ was observed (Table 5). The 1,003$cm^{-1}$ peak was chosen as a reference due to its proximity to the P–O stretch in HAP at 960 $cm^{-1}$ and because this peak does not overlap other nearby peaks that might confound the measured intensity (Schwartz et al. 2012). Nevertheless, these rises in the spectral ratio reflect increases in relative mineral concentration in the tissue but do not account for changes in the total amount of extracellular matrix (Schwartz et al. 2012). The clinical significance of this outcome is that the mineral gradient is a consistent feature of the mineralization growth front.

The Raman image based on the peak ratios of $CO_3^{2-}$ (carbonate) at 1,072 $cm^{-1}$ to $PO_4^{3-}$ (phosphate) at $\sim$ 960 $cm^{-1}$ (gradient of mineral content –GMC-) was obtained to measure the relative composition differences in the mineral and clearly determined the average degree of carbonate substitution in apatite (Schwartz et al. 2012). In general, the gradient of mineral content showed a reduction when loading was applied in dentin interfaces obtained with PA etching (Table 2). This finding implies lower carbonate/phosphate content at both HL ($\sim$ 43 %) and BHL ($\sim$ 52 %), after mechanical stimuli. The lowest values for the ratios were shown in loading square, as a result of new mineral extrafibrillar deposition, forming HAP, at the interface layer. Changes in the spectral region of carbonate content have been ascribed to either growth of a carbonate peak or changes in the phosphate peak in response to the presence of carbonate in the lattice (Awonusi et al. 2007). EDTA+SB samples showed a dissimilar performance, with increased (e.g., square at HL), decreased (e.g., hold 24 h at HL) or unchanged ratios (e.g., sine at BHL) (Table 4).

**Table 5** Organics and adhesive gradients in EDTA-treated dentin surfaces plus Single Bond (SB) adhesive application (EDTA + SB)

| | Normalization | Organics | | | | | | | | | Adhesive | | | | |
|---|---|---|---|---|---|---|---|---|---|---|---|---|---|---|---|
| | Crosslinking | | | | | Nature of collagen | | | | α-helices [1340] | DC [1637/1608] | Bis-GMA penetration [1113/amide I] | Adhesive penetration [1453/1667] | 1720 | 1453 |
| | Phenyl [1003] | Pyrid. [1032] | Ratio [1031/1001] | Ratio [1660/1690] | Ratio phenyl/$CH_2$ [1003/CH] | A-III [1246–1270] | CH [1450] | A-I [1655–1667] | Ratio amide I/amide III | | | | | | |
| *Unloading* | | | | | | | | | | | | | | | |
| ADH | 3.58 | 2.68 | 3.54 | 0.15 | 0.17 | 15.05 | 21.3 | 1.03 | 0.07 | 3.15 | 0.36 | 19.23 | 20.68 | 5.97 | 21.3 |
| HL | 3.51 | 4.64 | 1.31 | 0.39 | 0.22 | 12.74 | 15.86 | 1.86 | 0.15 | 3.95 | 0.63 | 6.12 | 8.53 | 3.7 | 15.86 |
| BHL | 4.77 | 6.24 | 1.3 | 1.1 | 0.57 | 13.22 | 8.37 | 4.69 | 0.35 | 5.16 | 1.82 | 1.06 | 1.78 | 1.57 | 8.37 |
| DEN | 7.6 | 10.22 | 1.34 | 1.3 | 0.79 | 4.37 | 9.62 | 5.66 | 1.3 | 5.20 | 2.23 | 1.08 | 1.7 | 1.31 | 9.62 |
| *Sine* | | | | | | | | | | | | | | | |
| HL | 15.01 | 11.63 | 0.77 | 0.64 | 0.44 | 23.26 | 34.2 | 10.66 | 0.46 | 19.04 | 0.87 | 1.5 | 3.2 | 14.62 | 34.2 |
| BHL | 5.35 | 3.86 | 0.72 | 0.74 | 0.28 | 18.73 | 19.17 | 6.4 | 0.34 | 17.54 | 1.61 | 0.56 | 3.0 | 8.88 | 19.17 |
| *Square* | | | | | | | | | | | | | | | |
| HL | 2.82 | 2.60 | 0.92 | 0.34 | 0.08 | 7.93 | 11.86 | 1.62 | 0.2 | 9.45 | 0.73 | 4.98 | 7.32 | 3.61 | 11.86 |
| BHL | 2.31 | 3.16 | 1.37 | 0.72 | 0.35 | 8.1 | 6.56 | 3.18 | 0.39 | 11.19 | 1.95 | 1.22 | 2.06 | 2.23 | 6.56 |
| *Hold 24 h* | | | | | | | | | | | | | | | |
| HL | 4.37 | 7.33 | 1.68 | 0.72 | 0.1 | 27.27 | 43.42 | 1.55 | 0.06 | 13.67 | 0.33 | 19.42 | 28.01 | 8.13 | 43.42 |
| BHL | 6.09 | 12.66 | 2.09 | 1.2 | 0.24 | 29.12 | 25.38 | 5.48 | 0.18 | 16.03 | 1.28 | 2.36 | 4.63 | 2.57 | 25.38 |
| *Hold 72 h* | | | | | | | | | | | | | | | |
| HL | 3.53 | 4.44 | 1.26 | 0.94 | 0.36 | 17.53 | 9.9 | 3.36 | 0.19 | 11.19 | 1.75 | 1.86 | 2.95 | 1.56 | 9.9 |
| BHL | 5.72 | 8.6 | 1.5 | 1.29 | 0.53 | 19.48 | 10.72 | 5.77 | 0.3 | 12.36 | 2.71 | 1.02 | 1.85 | 1.36 | 10.72 |

*Pyrid.* Pyridinium, *DC* degree of conversion of adhesive, *A-* amide, *ADH* adhesive, *BHL* bottom of hybrid layer, *HL* hybrid layer, *DEN* dentin. Peaks positions are expressed in $cm^{-1}$

On the other hand, the phosphate Raman peak intensities have been reported as a suitable parameter to detect differences between intact and demineralized substratum regions (Milly et al. 2014). In general, lower values of PPR (phosphate peak ratio) were obtained at HL than at BHL in all groups, except in loading square (Table 2), as the removal of HAP was more effective on superficial dentin, diminishing the phosphate groups and so the quotient, i.e., the ratio (Toledano et al. 2013). Overall, it was a considerable increase at HL (~ 75 %), and a drop at BHL (~ 90 %), in PPR, in all mechanical tests performed in PA + SB samples. EDTA + SB samples showed a unequal performance, with increased (e.g., sine at HL), decreased (e.g., square at HL) or unchanged ratios (e.g., sine at BHL).

After mechanical loading stimuli, remarkable changes in protein-derived peaks (900–1,800 $cm^{-1}$) were produced and displayed in Tables 3 and 5. A temporal correlation of transition between mineral and organic (1,004, 1,340 and 1,660 $cm^{-1}$) peaks has been advocated to play a direct role in mineral crystal nucleation and propagation within the growing mineral, though other Raman spectral bands (e.g., 1,243 $cm^{-1}$) did not change substantially during the mineralization process; this may lead to the assumption that nucleation and propagation of HAP is a multistep process involving both Young's modulus and mineral crystal transition (Wang et al. 2009).

The Raman band around 1,032 $cm^{-1}$ is assigned to the pyridinium ring vibration, which has a trivalent amino acid crosslinking residue (Daood et al. 2013). The pyridinium crosslink comes from the spontaneous reaction of keto-amines, immature crosslinks, which are formed via the action of lysyl oxidase and lysyl hydroxylases (Saito et al. 2006), and becomes a rapid screening method to check the crosslinking capability of collagen (Xu and Wang 2011), as the relative intensity of this peak increases after the crosslinking formation (Toledano et al. 2013). In general, mechanical loading in PA + SB samples may have stimulated the conversion of keto-amines, promoting a sharper and accentuated peak with a notable shift at 1,032 $cm^{-1}$, at both HL (~ 50 % increment), and BHL (~ 11 % increment) (except in square and hold 24 h) (Table 3). This high relative intensity of the peak corresponding to the pyridinium ring was associated with a nonreducible crosslinking formation, demonstrating that the first remineralization is intrafibrillar, due to the clear and well-defined spectra of crystallinity which reflects the Table 2, confirming that collagen is an active scaffold facilitating the formation of oriented crystalline hydroxyapatite inside the fibrils (Nudelman et al. 2010; Cölfen 2010). In EDTA + SB samples, the intensity of pyridinium ring increased at HL in loading in sine (Fig. 3b) and hold 24 h, and at BHL, when loading in hold (Table 5) (Fig. 3d, e). Collagen crosslinking is affected by tissue maturation as well as degree of mineralization, providing information about the structure and molecular interactions of complexes biomolecules (Xu and Wang 2011; Saito et al. 2006). This assertion was confirmed, e.g., by the high 1,032 $cm^{-1}$ intensity in hold 72 at BHL (7.33) (Table 3), relative high RMC (16.91) (Table 2) and high Young's modulus (Toledano et al. 2014c) in PA + SB.

The ratio 1,032 $cm^{-1}$/1,003 $cm^{-1}$ can be used, additionally, to measure the crosslinking reaction of collagen; the higher the ratio is, the greatest the extend of collagen crosslinking (Xu and Wang 2012). In our study, this ratio augmented in all mechanical loading tests when PA + SB was assessed (~ 196 % at HL and ~ 47 % at BHL), except at BHL in loading square (0.69) (Fig. 2c), but at HL, this test attained the maximum ratio (2.81) (Table 3). When EDTA was used as etching agent, this ratio dropped after mechanical stimuli in all tests (~ 13 %), except in loading hold 24 h (Fig. 3d). At BHL, this ratio augmented after loading (~ 9 %), except when cycling in sine, which decreased (Table 5). PA + SB, showed an increase in the ratio 1,660 $cm^{-1}$/1,690$cm^{-1}$ at HL with mechanical loading, and a general decrease at BHL, as occurred in hypermineralized substrates (Karan et al. 2009). On the other hand, when EDTA was used as etchant the relation between both peaks performed dissimilar, indicating mineralization at HL in loading square and at BHL in both loading in sine and square. Complementarily, mechanical loading promoted, at HL in PA + SB, a drop in the ratio 1,004 $cm^{-1}$/1,450$cm^{-1}$. At BHL, the ratio augmented in sine and hold 24 h, and decreased in square (Table 3). EDTA + SB promoted deposition of HAP, at HL in loading sine and hold 72 h, as the ratio 1,004 $cm^{-1}$/1,450 $cm^{-1}$ augmented (Table 5) (Wang et al. 2009). In addition to this, collagen crosslinking effect improved mechanical strength and stability of dentin collagen (Xu and Wang 2012) prevented not only collapse of collagen in the initial phases of the adhesive procedure (Daood et al. 2013), but permitted the growing of minerals within the demineralized dentin, as three-dimensional structures supporting effective mineralization may be created between intrafibrillar collagen molecules via the creation of specific crosslink formation that guide proper mineralization (Saito et al. 2006). Furthermore, it could be considered as another efficient biochemical way to block collagen from degradation (Xu and Wang 2011).

Confocal Raman spectroscopy evaluation supporting protein structural or conformational changes associated with mineralization can be elucidated from results reflected in Tables 2, 3, 4 and 5. The amide III band originates from the NH in plane deformation at 1,279 $cm^{-1}$ coupled to the CN stretching mode at 1,246 $cm^{-1}$ (Jastrzebska et al. 2003). Peaks corresponding to amide III (1,246–1,279 $cm^{-1}$) increased, in PA + SB after mechanical loading in all tests (~ 14 % at HL), except in hold 24 h (Table 3) (Fig. 2d) and loading square (Fig. 2c) when EDTA was used as etchant (Table 5). Similarly, amide I (1,655–1,667 $cm^{-1}$) in PA + SB

not only did not decrease its peak after mechanical loading challenge (Xu and Wang 2012), but drastically increased at HL in all groups (~ 300 %) and at BHL decreased in hold (Table 3) (Fig. 2d, e). In EDTA + SB, amide I increases in all tests, except in loading square and hold 24 h at HL (Table 5) (Fig. 3c, d). The new amine groups can be associated or linked with quite a few reactions like protein crosslinking (additionally amplified by the acidic nature of etched dentin) and nonenzymatic reactions of these free amino groups and sugars on proteins further leading to crosslinking (Daood et al. 2013). The spectral region of amide I was thought to be the best possible region for investigating the protein structure changes (Karan et al. 2009). The main contribution to the amide I band is the peptide carbonyl stretching vibration (Jastrzebska et al. 2003). Nevertheless, the amide I and amide III shift for crosslinked dentin specimens moved toward lower frequencies, denoting a declined crosslinking of collagen that results after nucleation. PA + SB loading in hold 24 h presented the lowest values of amide III, and lower Young's modulus results than hold 72 h (Toledano et al. 2014c), which showed higher peak of amide III (Table 3) and high values of crystallinity (Table 2). This combination of outcomes correlates well with a more advanced status of crystal maturity. $CH_2$ deformation vibration (1,450 $cm^{-1}$) augmented at HL in sine and square and at BHL in sine, in samples treated with PA (Table 3). EDTA-treated specimens showed an increment at HL when loading in sine and hold 24 h (Table 5) (Fig. 3b, d). These changes correspond with conformational changes in polypeptide chains (Xu and Wang 2011), which are associated with remineralization (Karan et al. 2009). Nevertheless, this peak of dentin is overlapped with the peak of the adhesive (Xu and Wang 2012), though the amide I (1,655–1,667 $cm^{-1}$) and III (1,246–1,270 $cm^{-1}$) peaks are not covered and are still distinguishable from the interface spectrum. Ratios of the amides I to III were higher when mineralization increased, as was reflected in Table 2 (~ 222 % at HL), attaining the highest values in loading in sine, at both HL and BHL; the lowest values (though superior to the unloaded specimens) were recorded in loading in hold, 72 h for PA + SB specimens (Table 3). EDTA-treated samples showed augmented ratios at HL in all tests (~ 53 %), except in hold 24 h; at BHL, the ratio only increased in loading square (Table 5).

In PA-treated specimens, the band centered at 1,340 $cm^{-1}$ (Fig. 2b) increased in all tests, except in hold 72 h, at both HL and BHL. At his wave, this tracing line exhibited a very low level of noise of fluctuation (Fig. 2c–e). Interestingly, this orientation-sensitive signal decreased when mineralization was allowed to proceed (Wang et al. 2009), corroborated by the high Young's modulus values that obtained in previous work (Toledano et al. 2014c). It is noteworthy that the protein-dependent spectral signal at α-helices (1,340 $cm^{-1}$) in hold 72 h, at HL (Fig. 2e), shows a peak of 3.99 (the lowest) and some of the highest peaks in both 960 $cm^{-1}$ (phosphate) (41.29) and 1,070 $cm^{-1}$ (carbonate) (8.18) (Tables 2, 3). Therefore, it can be assumed that this decrease (α-helices) precedes the appearance of HAP. In EDTA-treated samples, α-helices peaks incremented in all mechanical stimuli tests (Table 5) (~ 237 % at HL and ~ 177 % at HL). Therefore, confocal laser Raman spectroscopy has corroborated that growing of HA crystals within the resin–dentin interface is a multistep process involving both protein and mineral crystal transition.

The degree of conversion (DC) of adhesive (ratio 1,637 $cm^{-1}$/1,608 $cm^{-1}$), when PA was used as conditioning, augmented after mechanical loading, at both HL and BHL, except in hold 72 h, at BHL (Fig. 2e); loading in square attained the highest values at both HL and BHL (Table 3). When EDTA was applied as etching agent, DC increased in all mechanical tests, except in hold 24 h; this group, in junction with loading in sine, displayed the lowest ratio at BHL (Table 5). Nevertheless, the Bis-GMA penetration in PA + SB (ratio1113 $cm^{-1}$/1,667 $cm^{-1}$) and the adhesive (Bis-GMA and HEMA) penetration (ratio 1454 $cm^{-1}$/1,667 $cm^{-1}$) decreased, in general, in all mechanical loading tests as a consequence of the increase in amide I intensity (Table 3). Those ratios only incremented at BHL in hold 72 h and hold 24 and 72 h, respectively, as result of the decrement in the amide I band (Table 3) (Fig. 2d, e). In EDTA + SB, both ratios (1,113 $cm^{-1}$/1,667$cm^{-1}$, and ratio1454 $cm^{-1}$/1,667 $cm^{-1}$, Bis-GMA and adhesive penetration, respectively), reflected a general augmentation at BHL (except in sine and hold 72 h) and a decrease at HL (except in hold 24 h). Complementarily, the difference in the ratios of 1,454 $cm^{-1}$/1,667 $cm^{-1}$ and 1,113 $cm^{-1}$/1,667$cm^{-1}$ from HL toward BHL in the unloaded specimens indicated less diffusion across the interface, confirming that the resin–dentin interface is not impervious network, but a porous web and that the composition of this web is predominantly HEMA, with a lesser contribution from the BisGMA components (Wang and Spencer 2003). The peak at 1,720 $cm^{-1}$ is associated at carbonyl group. In PA + SB, this peak increased when loading in sine and square, at both HL and BHL (Table 3) (Fig. 2b, c). The reduced relative intensity of this band when loading in hold indicates less diffusion of resin monomers into the zone of demineralized dentin at the resin–dentin interface (Wang and Spencer 2003). In EDTA + SB, this peak increased at HL in sine and hold 24 h (Fig. 3b, d); at BHL its intensity increased in all mechanical tests, except in hold 72 h, at BHL (Table 5). The peak at 1,453 $cm^{-1}$ is associated at $CH_2$ def (Xu and Wang 2012; Wang and Spencer 2003), (C-H alkyl group) and denoted a measure of both the organic components and the resin adhesive, at the interface (Daood et al. 2013). In PA + SB, this peak increased when loading in sine and square, at HL, and at BHL when loading in sine (Table 3) (Fig. 2b, c). In EDTA + SB, the increase affected to loading in sine and hold 24 h, at HL

(Fig. 3b, d). At BHL, the peak only decreased when loading in square (Table 5; Fig. 3c).

From the results reported in the present work and related outcomes reported (Toledano et al. 2014c), it can be assumed that (1) interfaces originated after phosphoric acid (PA) conditioning and further adhesive application presented and advanced degree of mineralization as a consequence of, (i) high level of relative presence of minerals and their ratios of mineral content (RMC), specially phosphate group and its influence on the gradient of mineral content (GMC), and the ratio of phosphate peak (PPR), (ii) high crystallinity (lower FWHM), specially concerning the phosphate groups, (iii) high or low values of crosslinking measurements, depending on the ratios, reflecting mineralization, and (iv) the parameters describing the nature of collagen, where the general increase in peaks (amide III/I and their ratio, and CH support the mineralization increase; additionally, the α-helices signal decreased when mineralization was allowed to proceed, attaining the lowest peak and the maximum values of nanomechanical properties (Toledano et al. 2014c) at both hybrid layer (HL) and bottom of hybrid layer (BHL) when loading in hold 72 h, showing a more advanced stage of mineralization. (2) Interfaces originated after EDTA conditioning and further adhesive application are prone to be conducting a more delayed but mature procedure of dentin mineralization. Several reasons may be advocated, (i) values concerning the relative presence of minerals parameters only increased in some groups, (ii) generalization of low crystallinity, concerning both minerals, (iii) dissimilar performance in crosslinking and nature of collagen measurements, indicating that the deposit of minerals is a sequential and unfinished biological procedure (Osorio et al. 2014), in this test and, (iv) the α-helices signal increased in all groups.

Compressive load stimulates the alkaline phosphatase in vivo and in vitro (McAllister and Frangos 1999), producing free phosphate (Posner et al. 1986). EDTA-treated samples showed greatest phosphate signals, especially when loading in hold (Tables 2, 4). At high phosphate concentration, calcium pyrophosphate, calcium phosphate and unstable and noncrystalline amorphous complexes are formed (Cheng and Pritzker 1983). Conversely, inorganic pyrophosphate is a potent inhibitor of the hydroxyapatite (HAP) crystal growth (Rodrigues et al. 2011). EDTA-treated samples showed the lowest crystallinity parameter (Tables 2, 4). Moreover, the use of mild or neutral etching agents leave a substantial amount of HAP around the collagen fibrils keeping the alkaline phosphatase and other enzymes "fossilized" (Van Meerbeek et al. 2011), thus hindering the complete remineralization. On the contrary, PA etching freed them from their "fossilized" state, contributing to some more advanced remineralization, as crystallinity was shown to increase in PA + SB specimens (Table 2).

Dentin remodeling is dependent on the dentin's loading history resulting, after restoration, in a resin–dentin structure capable of functional load bearing. To characterize the sequential phases of dentin remineralization and its effect on the three main components of the interface (mineral, matrix and resin) may pose a challenge for future dental interventionist therapies.

## 4 Conclusions

Results of the present work demonstrated that when phosphoric acid (PA) was used as conditioning agent, loading in square waveform promoted the highest dentin mineralization degree, based on the increase in the relative presence of minerals and crystallinity of, specially, the phosphate group. When the conditioning agent was EDTA, loading in hold waveform 72 h promoted the highest mineralization at the hybrid layer and at the bottom of the hybrid layer when loading in hold 24 h; this new mineral did not achieve any more advance crystallographic maturity in relation with the phosphate group. High crosslinking parameters and conformational changes in proteins associated regularly with high ratios of remineralization in dentin surfaces conditioned with PA, indicating that the first remineralization is intrafibrillar. Crosslinking and protein structures in specimens treated with EDTA performed dissimilar, presenting different phases of dentin mineralization. Mechanical loading, in addition, promoted a generalized increase in the degree of cure of the adhesive.

**Acknowledgments** This work was supported by Grants CICYT/FEDER MAT2011-24551, JA-P08-CTS-3944 and CEI-Biotic UGR. The authors have no financial affiliation or involvement with any commercial organization with direct financial interest in the materials discussed in this manuscript. Any other potential conflict of interest is disclosed.

## References

Almahdy A, Downey FC, Sauro S, Cook RJ, Sherriff M, Richards D, Watson TF, Banerjee A, Festy F (2012) Microbiochemical analysis of carious dentin using Raman and fluorescence spectroscopy. Caries Res 46:432–440

Awonusi A, Morris MD, Tecklenburg MM (2007) Carbonate assignment and calibration in the Raman spectrum of apatite. Calcif Tissue Int 81:46–52

Balooch M, Habelitz S, Kinney JH, Marshall SJ, Marshall GW (2008) Mechanical properties of mineralized collagen fibrils as influenced by demineralisation. J Struct Biol 162:404–410

Cheng PT, Pritzker KP (1983) Pyrophosphate, phosphate ion interaction: effects on calcium pyrophosphate and calcium hydroxyapatite crystal formation in aqueous solutions. J Rheumatol 10:769–777

Cölfen H (2010) Biomineralization: a crystal-clear view. Nat Mater 9:960–961

Daood U, Iqbal K, Nitisusanta LI, Fawzy AS (2013) Effect of chitosan/riboflavin modification on resin/dentin interface: spectroscopic and microscopic investigations. J Biomed Mater Res A 101:1846–1856

De Munck J, Van Landuyt K, Peumans M, Poitevin A, Lambrechts P, Braem M et al (2005) A critical review of the durability of adhesion to tooth tissue: methods and results. J Dent Res 84:118–132

Erickson RL (1992) Surface interactions of dentin adhesive materials. Oper Dent Suppl 5:81–94

Frankenberger R, Pashley DH, Reich SM, Lohbauer U, Petschelt A, Tay FR (2005) Characterisation of resin-dentine interfaces by compressive cyclic loading. Biomaterials 26:2043–2052

Jastrzebska M, Wrzalik R, Kocot A, Zalewska-Rejdak J, Cwalina B (2003) Raman spectroscopic study of glutaraldehyde-stabilized collagen and pericardium tissue. J Biomater Sci Polym Ed 14:185–197

Karan K, Yao X, Xu C, Wang Y (2009) Chemical profile of the dentin substrate in non-carious cervical lesions. Dent Mater 25:1205–1212

Kinney JH, Habelitz S, Marshall SJ, Marshall GW (2003) The importance of intrafibrillar mineralization of collagen on the mechanical properties of dentin. J Dent Res 82:957–961

Koibuchi H, Yasuda N, Nakabayashi N (2001) Bonding to dentin with a self-etching primer: the effect of smear layers. Dent Mater 17: 122–126

Krajewski A, Mazzocchi M, Buldini PL, Ravaglioli A, Tinti A, Taddei P, Fagnano C (2005) Synthesis of carbonated hydroxyapatites: efficiency of the substitution and critical evaluation of analytical methods. J Mol Struct 744–747:221–228

Marshall GW Jr, Inai N, Wu-Magidi IC, Balooch M, Kinney JH, Tagami J, Marshall SJ (1997) Dentin demineralization: effects of dentin depth, pH and different acids. Dent Mater 13:338–343

McAllister TN, Frangos JA (1999) Steady and transient fluid shear stress stimulate NO release in osteoblasts through distinct biochemical pathways. J Bone Miner Res 14:930–936

Milly H, Festy F, Watson TF, Thompson I, Banerjee A (2014) Enamel white spot lesions can remineralise using bio-active glass and polyacrylic acid-modified bio-active glass powders. J Dent 42:158–66

Nakabayashi N (1992) The hybrid layer: a resin-dentin composite. Proc Finn Dent Soc 88(Suppl 1):321–329

Nishigawa K, Bando E, Nakano M (2001) Quantitative study of bite force during sleep associated bruxism. J Oral Rehabil 28:485–491

Noma N, Kakigawa H, Kozono Y, Yokota M (2007) Cementum crack formation by repeated loading in vitro. J Periodontol 78:764–769

Nudelman F, Pieterse K, George A, Bomans PH, Friedrich H, Brylka LJ, Hilbers PA, De With G, Sommerdijk NA (2010) The role of collagen in bone apatite formation in the presence of hydroxyapatite nucleation inhibitors. Nat Mater 9:1004–1009

Osorio R, Erhardt MC, Pimenta LA, Osorio E, Toledano M (2005) EDTA treatment improves resin-dentin bonds' resistance to degradation. J Dent Res 84:736–740

Osorio R, Osorio E, Cabello I, Toledano M (2014) Zinc induces apatite and scholzite formation during dentin remineralization. Caries Res 48:276–290

Posner AS, Blumenthal NC, Boskey AL (1986) Model of aluminum-induced osteomalacia: inhibition of apatite formation and growth. Kidney Int (Suppl) 18:S17–S19

Rodrigues TL, Nagatomo KJ, Foster BL, Nociti FH, Somerman MJ (2011) Modulation of phosphate/pyrophosphate metabolism to regenerate the periodontium: a novel in vivo approach. J Periodontol 82:1757–1766

Saito M, Fujii K, Marumo K (2006) Degree of mineralization-related collagen crosslinking in the femoral neck cancellous bone in cases of hip fracture and controls. Calcif Tissue Int 79:160–168

Sano H, Yoshikawa T, Pereira PN, Kanemura N, Morigami M, Tagami J, Pashley DH (1999) Long-term durability of dentin bonds made with a self-etching primer, in vivo. J Dent Res 78:906–911

Sauro S, Mannocci F, Toledano M, Osorio R, Pashley DH, Watson TF (2009) EDTA or H3PO4/NaOCl dentin treatments may increase hybrid layers' resistance to degradation: a microtensile bond strength and confocal-micropermeability study. J Dent 37:279–288

Schwartz AG, Pasteris JD, Genin GM, Daulton TL, Thomopoulos S (2012) Mineral distributions at the developing tendon enthesis. PLoS One 7:e48630

Simonsen RJ (1987) The preventive resin restoration: a minimally invasive, nonmetallic restoration. Compendium 8:428–430

Toledano M, Osorio E, Aguilera FS, Cabrerizo-Vílchez MA, Osorio R (2012a) Surface analysis of conditioned dentin and resin-dentin bond strength. J Adhes Sci Technol 26:27–40

Toledano M, Yamauti M, Ruiz-Requena ME, Osorio R (2012b) A ZnO-doped adhesive reduced collagen degradation favouring dentine remineralization. J Dent 40:756–765

Toledano M, Cabello I, Vílchez MA, Fernández MA, Osorio R (2013) Surface microanalysis and chemical imaging of early dentin remineralization. Microsc Microanal 25:1–12

Toledano M, Osorio E, Aguilera FS, Sauro S, Cabello I, Osorio R (2014a) In vitro mechanical stimulation promoted remineralization at the resin/dentin interface. J Mech Behav Biomed Mater 30:61–74

Toledano M, Aguilera FS, Cabello I, Osorio E, Osorio R (2014b) Load cycling enhances bioactivity at the resin-dentine interface. Dent Mater. doi:10.1016/j.dental.2014.02.009

Toledano M, Cabello I, Aguilera FS, Osorio E, Osorio R (2014c) Dentin mechano-transduction stimuli are associated with tissue remodeling. Microsc Microanal (in press)

Toledano M, Osorio E, Cabello I, Osorio R (2014d) Early dentine remineralisation: morpho-mechanical assessment. J Dent 42:384–394

Van Meerbeek B, Yoshihara K, Yoshida Y, Mine A, De Munck J, Van Landuyt KL (2011) State of the art of self etch adhesives. Dent Mater 27:17–28

Wang Y, Spencer P (2003) Hybridization efficiency of the adhesive/dentin interface with wet bonding. J Dent Res 82:141–145

Wang C, Wang Y, Huffman NT, Cui C, Yao X, Midura S, Midura RJ, Gorski JP (2009) Confocal laser Raman microspectroscopy of biomineralization foci in UMR 106 osteoblastic cultures reveals temporally synchronized protein changes preceding and accompanying mineral crystal deposition. J Biol Chem 284:7100–7113

Xu C, Wang Y (2011) Cross-linked demineralized dentin maintains its mechanical stability when challenged by bacterial collagenase. J Biomed Mater Res B Appl Biomater 96:242–248

Xu C, Wang Y (2012) Collagen cross linking increases its biodegradation resistance in wet dentin bonding. J Adhes Dent 14:11–18